MEANDROS MEDICAL AND DENTAL JOURNAL
March 2025 (1):117-128

Meandros Medical and Dental Journal
doi: 10.69601/meandrosmdj.1603483

Research Article

IMPACT OF DIFFERENT SUBSTRUCTURE AND SUPERSTRUCTURE MATERIALS ON BONE STRESS DISTRIBUTION IN ALL-ON-4 PROSTHETIC RESTORATIONS

Ege ÇOLAK[1]* , Muharrem Erhan ÇÖMLEKOĞLU[1], Mehmet SONUGELEN[1], Makbule Heval ŞAHAN[1]

[1]Department of Prosthodontics, Faculty of Dentistry, Ege University, Izmir, Turkey

*Correspondence: dt.egecolak@gmail.com

Abstract

Aim: This study aimed to examine whether different framework and superstructure materials in All-on-4 prosthetic restorations affect load distribution in peri-implant bone.

Materials and Methods: Four implants were placed according to the All-on-4 concept, with distal implants angled at 30 degrees. Framework materials (cobalt-chromium alloy, titanium, PEEK, zirconia) and superstructure materials (composite, zirconia) created eight combinations. 3D models were designed using Rhinoceros 4.0 (3670 Woodland Park Ave N, Seattle, Washington, USA) and VRMesh (VirtualGrid Inc, Bellevue City, Washington, USA), then imported into Algor Fempro (ALGOR, Inc., 150 Beta Drive, Pittsburgh, Pennsylvania, USA) for finite element analysis. A 150N force was applied perpendicular to the occlusal surfaces of the left first molar and premolar.

Results: The PEEK framework group showed the highest maximum principal stress (HMaxPS) values in the cortical bone (CB) near the applied force. The zirconia superstructure exhibited lower maximum principal stress values than the composite superstructure. Minimum principal stress (MinPS) was lower in the composite superstructure than in the zirconia superstructure. In the cantilever section, peak MinPS values in the cortical bone decreased as the elastic modulus of the frameworks increased, following the order: PEEK > titanium > Cr-Co > zirconia.

Conclusions: The PEEK framework and composite superstructure generated higher tensile forces in the cortical bone surrounding the implants. The highest compression values were observed in the PEEK framework, followed by titanium, Cr-Co, and zirconia. Greater stress accumulation occurred in the cortical bone with the composite superstructure compared to the zirconia superstructure.

Keywords: All-on-4, Framework, Finite Element Analysis

Received: *26 December 2024*
Revised: *12 February 2025*
Accepted: *23 February 2025*
Published: *20 March 2025*

MEANDROS MEDICAL AND DENTAL JOURNAL
March 2025 (1):117-128

Meandros Medical and Dental Journal
doi: 10.69601/meandrosmdj.1603483

INTRODUCTION

When planning dental implant placement in the edentulous mandible, reduced residual alveolar bone height due to bone resorption or anatomical limitations such as the mandibular canal can pose challenges, particularly in the posterior region. Long-term clinical data has demonstrated that fixed prostheses supported by four implants in the mandible exhibit similar prosthesis and implant survival rates as those supported by a greater number of implants (1). Increasing the number of implants is essential to reduce stress on implants and prosthetic components and ensure even load distribution on the underlying bone. However, in patients with severe alveolar bone loss, the area available for implant placement is limited. In some completely edentulous patients, implant-supported prostheses are almost impossible to fabricate without complex procedures such as nerve transposition, grafting in the posterior maxilla and mandible (2).

The All-on-4 concept has been introduced as an alternative to bone augmentation procedures. The All-on-4 concept, developed by Malo, is one of the most widely used methods for treating complete mandibular edentulism with angled implants. The All-on-4 concept involves placing four implants in the interforaminal region of the completely edentulous mandible followed by the use of a fixed prosthesis (1). The posterior implants are angled at 30 degrees to reduce cantilever length. The angulation of the posterior implants should not exceed 45 degrees (2). Distal angulation of the implants provides advantages such as the use of longer implants and better cortical support (3).

In full-mouth restorations, long spans can lead to more complications with the prosthetic substructure compared to short spans. A prosthesis spanning the entire arch may be subject to more deformation and bending. Therefore, cases with long spans may experience more stress. In cases with long spans, especially in the presence of cantilevers, the prosthetic substructure material becomes even more important in ensuring the stability of the system (4). Titanium alloys, cobalt-chromium, zirconia, and polyetheretherketone are frequently utilized in the manufacture of implant substructures (5).

Cobalt-chromium (Co-Cr) alloys can be defined as high-strength, non-magnetic, biocompatible alloys that are resistant to heat, wear, corrosion, and tarnishing. Thanks to their high elastic modulus, they provide the necessary strength and rigidity without the need to increase the material thickness and, consequently, the weight (6). Cobalt-chromium alloys are frequently used as prosthetic substructure materials in implant-supported prostheses due to their low cost, low density, and good mechanical properties (4).

Titanium is one of the most commonly used materials in the substructure of All-on-4 prostheses. This is due to its biocompatibility, low cost, and good mechanical properties (7). Titanium is a practical material for the production of implant-supported prosthetic substructures (8). CAD/CAM-manufactured titanium substructures have a high degree of fit in full-arch or partial-arch restorations. Titanium substructures can cause aesthetic complications due to their grayish color (9). They can cause metal allergies (10).

PEEK is a type of linear high-performance polymer due to its mechanical properties, high temperature stability, and chemical resistance. PEEK also has a tooth-like color, is lightweight, and is an alternative for patients with metal allergies (11). PEEK is an organic, thermoplastic, high-performance polymer. It is similar to human bone in terms of weight, strength, and other chemical properties (7). While the elastic modulus of metal substructures is between 100-200 GPa, that of PEEK is around 4 GPa. Despite this difference in the mechanical properties of these two materials, it is assumed that PEEK can be an alternative as a substructure material in implant-supported fixed prosthetic restorations (12).

Zirconia is the most preferred bioengineering ceramic among all ceramic products. With its excellent biocompatibility, low thermal conductivity, high flexural strength, and suitability for white aesthetics, it is an ideal material (13). The reason for its popularity in dentistry is its transformation toughening property. This property helps prevent crack propagation and increases localized fracture resistance. 3 mol% Y_2O_3 stabilized zirconia, or yttria-stabilized tetragonal zirconia polycrystal (3Y-TZP), is the most commonly preferred zirconia when a hard material is needed (13). The use of zirconia as a substructure material helps to mask the substructure color and has survival rates similar to metal (10). Zirconia can also be used as a superstructure material in All-on-4 prostheses.

Composites are among the materials used for veneering in implant-supported prostheses. Composites have advantages such as stress distribution, reduction of prosthesis weight, and reduction of treatment costs. They are a good alternative to porcelain in full-mouth implant-supported prosthetic restorations (9).

MEANDROS MEDICAL AND DENTAL JOURNAL
March 2025 (1):117-128

Meandros Medical and Dental Journal
doi: 10.69601/meandrosmdj.1603483

Finite element analysis (FEA) is a widely used, non-destructive computational approach for modeling and examining the mechanical behavior of systems under various conditions. By partitioning structures into discrete elements, this technique is applied in engineering and dentistry to assess both material performance and design efficacy (5). It is a useful approach because it allows for the unlimited repetition of experiments under different scenarios—experiments that cannot be exactly reproduced in clinical settings—and also makes it possible to conduct tests that cannot be performed on patients for ethical reasons, without bearing ethical responsibility. In implants, intermittent forces during oral functions lead to bone resorption by creating overload that results in high stress and strain, rather than insufficient mechanical stimulation of the bone. Since direct measurement of bone strain via strain gauge needles in patients is impractical, indirect mathematical approaches like FEA are frequently employed to calculate values such as strain, stress, and deformation.

The finite element analysis results provided valuable insights into stress distributions within the bone and implant components under various loading conditions. This information is crucial for the design and optimization of dental implants, aiming to improve their long-term performance and patient outcomes.

In our literature review, we did not encounter any study that simultaneously evaluates the relationship between substructure and superstructure in all-on-4 prostheses with a Toronto design and examines the resulting stress on the bone. Based on the results of our study, we may have a clinical prediction regarding which substructure and superstructure in all-on-4 prostheses could lead to less bone loss.

The null hypothesis of the study is that there is no difference in the effect of different substructure and superstructure materials used in All-on-4 prosthetic restorations on bone stress distribution.

MATERIALS AND METHODS

Software

This study utilized Rhinoceros 4.0 for 3D (3- dimension) modeling, VRMesh for mesh processing, and Algor Fempro for finite element analysis.

Implant and prosthetic Design

Conical implants at bone level were used in the study. Implants with a diameter of 4.1mm (millimeter) and a length of 12mm were selected. Four implants were positioned in the mandible: the anterior implants were placed vertically, and the posterior two implants were angled distally at 30°. The anterior implants were aligned with the lateral teeth, and the screw access points of the posterior implants aligned to the second premolar tooth. Multi-unit abutments were placed on the implants. The anterior multi-unit abutments were modeled without an angle, while the posterior two multi-unit abutments were modeled at a 30° angle to compensate for the implant angle. The prosthetic solution was planned as an All-on-4 prosthesis design. A prosthetic substructure was designed, and crowns were designed on top of the framework. The prosthetic substructures were made of cobalt-chromium alloy, titanium, PEEK, and zirconia. The prosthetic superstructures were made of composite and zirconia. A total of eight different combinations were obtained by using the substructures and superstructures together: cobalt-chromium substructure with composite superstructure, PEEK substructure with composite superstructure, titanium substructure with composite superstructure, zirconia substructure with composite superstructure, cobalt-chromium substructure with zirconia superstructure, PEEK substructure with zirconia superstructure, titanium substructure with zirconia superstructure, and zirconia substructure with zirconia superstructure.

The prosthetic restoration was designed with 12 teeth. The screw access holes opening to the occlusal surface of the distal implants were modeled to exit the occlusal surface of the second premolar tooth. The modeling was done so that the distance from the exit point of the screw holes to the distal surface of the first molar tooth (cantilever length) was 9mm. The distance between the line passing through the anterior implant and the line passing through the posterior implant was 9 mm. The cantilever length/anterior-posterior implant distance (A-P distance) ratio is 1.

Load Application

Forces were applied perpendicular to the occlusal surface of the left first molar tooth and the occlusal surface of the left first premolar tooth (Fig. 1 e,f). The force magnitude was 150N (Newton)(4).

This study employed a multi-stage computational approach for the finite element analysis of mandibular implants. A 3D scan of the mandible was acquired using an Activity 880 optical scanner. The acquired data was then processed on a workstation equipped with an Intel Xeon® R CPU 3.30 gigahertz processor, 500 gigabyte hard disk, 14 gigabyte RAM, and Windows 7 Ultimate operating system.

MEANDROS MEDICAL AND DENTAL JOURNAL
March 2025 (1):117-128

Meandros Medical and Dental Journal
doi: 10.69601/meandrosmdj.1603483

The initial 3D models of the mandible and prosthetic components were generated in VRMesh software. These models were subsequently exported in the industry-standard STL(Standard Triangle Language) format for compatibility with Algor Fempro, a finite element analysis software. STL format ensures the preservation of crucial node coordinate information during data transfer between different software packages.

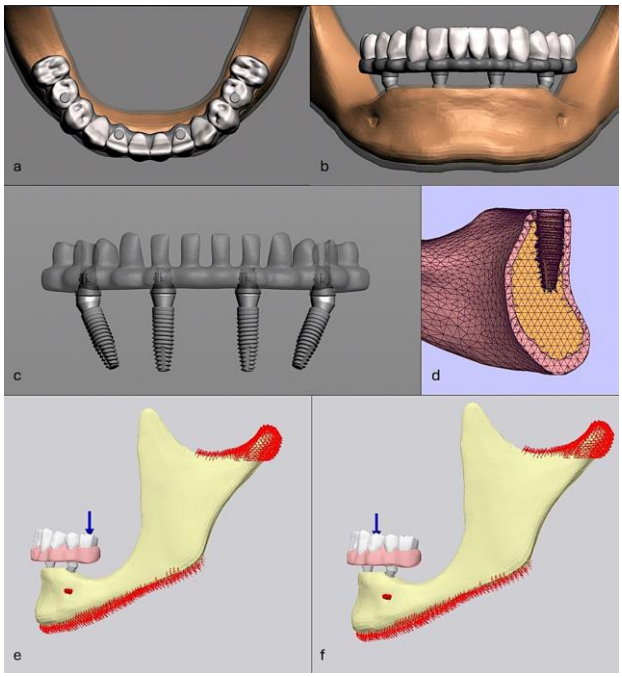

Figure 1. (a) Modeling from an occlusal view; (b) Modeling from a frontal view; (c) Model with the mandible separated and substructures faded; (d) Mesh view of implants within the mandible; (e, f) Force application to the left first molar (e) and the left first premolar (f).

Within Algor Fempro, the models were assigned appropriate material properties, including Young's Modulus and Poisson's ratio (Table 1), to accurately reflect the mechanical behavior of each component. Assuming linear elastic, homogeneous, and isotropic material behavior, the software proceeded with the meshing process.

To achieve optimal mesh quality, 8-node brick elements were predominantly used. In regions with complex geometries, elements with fewer nodes were incorporated to ensure complete mesh coverage. This approach aimed to balance mesh refinement with computational efficiency. Furthermore, sharp and narrow features within the jaw models, which can pose challenges for accurate analysis, were smoothed to improve mesh quality and stability.

Table 1. Material properties

Material	Young's Modulus (MPa)	Poisson's Ratio
Cortical Bone	13700	0.3
Spongy Bone	1370	0.3
Zirconia Substructure	210000	0.3
PEEK Substructure	4200	0.36
Titanium	110000	0.28
Composite	15000	0.24
Cr-Co Substructure	200000	0.3
Zirkonya Superstructure	213700	0.31

The number of elements within the finite element mesh was maximized within the computational constraints of the system (Table 2), considering the dimensions of the mandible model. This maximization aimed to enhance the accuracy of the subsequent stress analysis.

Table 2. Node and element numbers of substructure and superstructure combinations.

Combinations	Node Numbers	Element Numbers
Cr-Co Substructure – Composite Superstructure	470975	1932039
PEEK Substructure – Composite Superstructure	470975	1932050
Titanium Substructure –Composite Superstructure	470975	1932052
Zirconia Substructure – Composite Superstructure	470975	1932039
Cr-Co Substructure – Zirconia Superstructure	470975	1932039
PEEK Substructure – Zirconia Superstructure	470975	1932052
Titanium Substructure – Zirconia Superstructure	470975	1932050
Zirconia Substructure – Zirconia Superstructure	470975	1932052

Following the initial analysis in Algor Fempro, the models were further refined in Rhinoceros 4.0 3D Software. In this stage, prosthetic components such as screws, implants, and abutments were precisely aligned with the bone structures using Boolean operations, ensuring accurate representation of their spatial relationships.

Bone tissues were segmented based on Hounsfield units, a technique commonly used in medical imaging. The segmented regions were then rendered into a 3D model, and subsequently simplified using 3D-Doctor software to optimize model complexity and reduce computational demands. This simplified model served as a reference for

MEANDROS MEDICAL AND DENTAL JOURNAL
March 2025 (1):117-128

Meandros Medical and Dental Journal
doi: 10.69601/meandrosmdj.1603483

the creation of a new bone model, incorporating anatomical measurements from the Wheeler atlas.

The newly created bone model underwent dimensional and topographic adjustments in VRMesh software to achieve greater anatomical accuracy. Cancellous bone was extracted from the bone tissue using the offset method, allowing for the accurate representation of the distinct bone microstructures.

Finally, the refined models, including the mandible, prosthetic components, and bone tissues, were imported back into Algor Fempro for the final finite element analysis. Boundary conditions were applied to the model to simulate real-world constraints, such as fixation at the base of the mandible.

RESULTS

Results of maximum principal stress in cortical bone around the implant

In the Cr-Co substructure with a composite superstructure, when force was applied between the two implants, the highest MaxPS was observed in the CB of the left anterior implant region at 4.699767 N/mm², while the lowest was found in the CB of the right anterior implant region at 1.453774 N/mm² (Fig.2a) (Table 3). When force was applied to the cantilever portion of the same combination, the highest MaxPS was found in the CB of the right anterior implant region at 19.011616 N/mm², and the lowest in the CB of the right posterior implant region at 4.401233 N/mm² (Fig.2b)(Table 3).

In the PEEK substructure with a composite superstructure, when force was applied between the two implants, the highest MaxPS was observed in the CB of the left anterior implant region at 6.299223 N/mm², while the lowest was found in the CB of the right posterior implant region at 2.757486 N/mm² (Fig.2c) (Table 3). When force was applied to the cantilever portion of the same combination, the highest MaxPS was found in the CB of the left posterior implant region at 12.984744 N/mm², and the lowest in the CB of the right posterior implant region at 2.373965 N/mm² (Fig2d) (Table 3).

In the titanium substructure with a composite superstructure, when force was applied between the two implants, the highest MaxPS was observed in the CB of the left anterior implant region at 4.930487 N/mm², while the lowest was found in the CB of the right anterior implant region at 1.522162 N/mm² (Fig.2e) (Table 3). When force was applied to the cantilever portion of the same combination, the highest MaxPS was found in the CB of the right anterior implant region at 18.022934 N/mm², and the lowest in the CB of the right posterior implant region at 4.066457 N/mm² (Fig.2f) (Table 3).

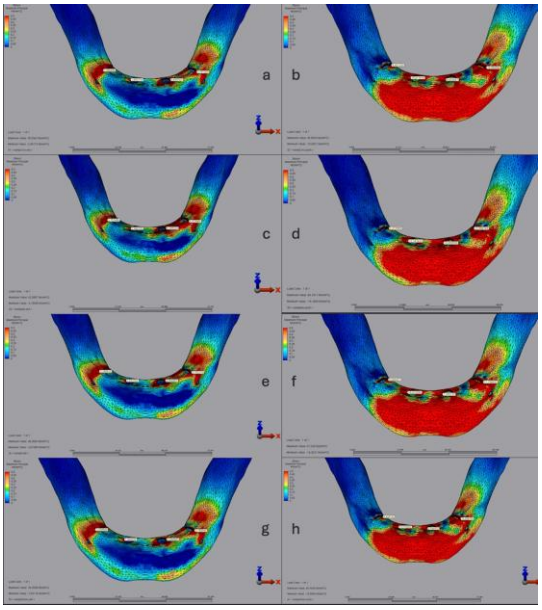

Figure 2. Composite Superstructure Maximum Principal Stress; (a, b) Cr-Co Substructure (a: anterior load, b: posterior load); (c, d) PEEK Substructure (c: anterior load, d: posterior load); (e, f) Titanium Substructure (e: anterior load, f: posterior load); (g, h) Zirconia Substructure (g: anterior load, h: posterior load).

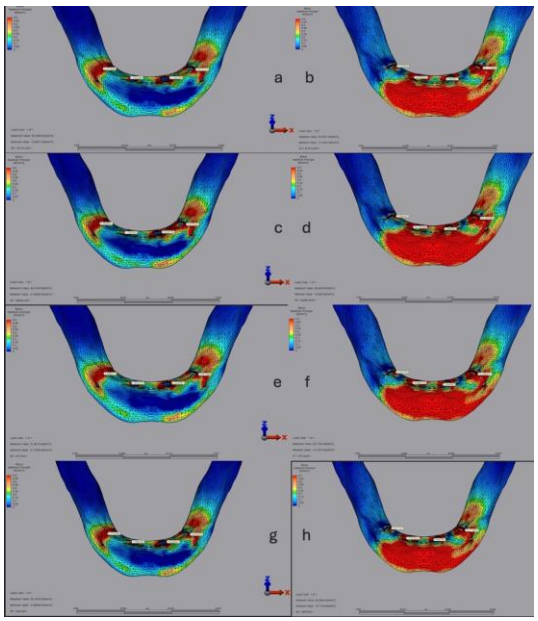

Figure 3. Zirconia Superstructure Maximum Principal Stress; (a, b) Cr-Co Substructure (a: anterior load, b: posterior load); (c, d) PEEK Substructure (c: anterior load, d: posterior load); (e, f) Titanium Substructure (e: anterior load, f: posterior load); (g, h) Zirconia Substructure (g: anterior load, h: posterior load).

MEANDROS
MEDICAL AND DENTAL JOURNAL
March 2025 (1):117-128

Table 3. Maximum principal stress (MaxPS) values (N/mm²) in cortical bone around the implant for different substructure and superstructure combinations.

Combination	Anterior load – Right posterior implant	Anterior load – Right anterior implant	Anterior load – Left anterior implant	Anterior load – Left posterior implant	Posterior load – Right posterior implant	Posterior load – Right anterior implant	Posterior load – Left anterior implant	Posterior load – Left posterior implant
Cr-Co Substructure-Composite Superstructure	3.356658	1.453774	4.699767	3.791263	4.401233	19.011616	6.642647	10.954504
PEEK Substructure-Composite Superstructure	2.757486	2.984783	6.299223	4.523866	2.373965	12.141423	10.093930	12.984744
Titanium Substructure- Composite Superstructure	3.299923	1.522162	4.930487	3.752276	4.066457	18.022934	7.205133	11.136632
Zirconia Substructure-Composite Superstructure	3.359844	1.449526	4.680983	3.789548	4.424193	19.078002	6.594923	10.936705
Cr-Co Substructure -Zirconia Superstructure	3.377530	1.493344	4.106259	3.872213	4.323566	19.839220	4.880561	10.127559
PEEK Substructure-Zirconia Superstructure	3.383961	1.209262	5.028194	3.915142	3.998480	18.166266	7.359382	10.497856
Titanium Substructure-Zirconia Superstructure	3.405513	1.452275	4.242281	3.851988	4.329700	19.868105	5.304943	10.266977
Zirconia Substructure-Zirconia Superstructure	3.374380	1.496259	4.095691	3.874375	4.321727	19.824913	4.846240	10.113878

In the zirconia substructure with a composite superstructure, when force was applied between the two implants, the highest MaxPS was observed in the CB of the left anterior implant region at 4.680983 N/mm², while the lowest was found in the CB of the right anterior implant region at 1.449526 N/mm² (Fig.2g) (Table 3). When force was applied to the cantilever portion of the same combination, the highest MaxPS was found in the CB of the right anterior implant region at 19.078002 N/mm², and the lowest in the CB of the right posterior implant region at 4.424193 N/mm² (Fig2h) (Table 3).

In the Cr-Co substructure with a zirconia superstructure, when force was applied between the two implants, the highest MaxPS was observed in the CB of the left anterior implant region at 4.106259 N/mm², while the lowest was found in the CB of the right anterior implant region at 1.493344 N/mm² (Fig.3a) (Table 3). When force was applied to the cantilever portion of the same combination, the highest MaxPS was found in the CB of the right anterior implant region at 19.839220 N/mm², and the lowest in the CB of the right posterior implant region at 4.323566 N/mm² (Fig.3b) (Table 3).

In the PEEK substructure with a zirconia superstructure, when force was applied between the two implants, the highest MaxPS was observed in the CB of the left anterior implant region at 5.028194 N/mm², while the lowest was found in the CB of the right anterior implant region at 1.209262 N/mm² (Fig.3c) (Table 3). When force was applied to the cantilever portion of the same combination, the highest MaxPS was found in the CB of the right anterior implant region at 18.166266 N/mm², and the lowest in the CB of the right posterior implant region at 3.998480 N/mm² (Fig.3d) (Table 3).

In the titanium substructure with a zirconia superstructure, when force was applied between the two implants, the highest MaxPS was observed in the CB of the left anterior implant region at 4.242281 N/mm², while the lowest was found in the CB of the right anterior implant region at 1.452275 N/mm² (Fig.3e) (Table 3). When force was applied to the cantilever portion of the same combination, the highest MaxPS was found in the CB of the right anterior implant region at 19.868105 N/mm², and the lowest in the CB of the right posterior implant region at 4.329700 N/mm² (Fig.3f) (Table 3).

In the zirconia substructure with a zirconia superstructure, when force was applied between the two implants, the highest MaxPS was observed in the CB of the left anterior implant region at 4.095691 N/mm², while the lowest was found in the CB of the right anterior implant region at

MEANDROS MEDICAL AND DENTAL JOURNAL
March 2025 (1):117-128

Meandros Medical and Dental Journal
doi: 10.69601/meandrosmdj.1603483

1.496259 N/mm² (Fig.3g) (Table 3). When force was applied to the cantilever portion of the same combination, the highest MaxPS was found in the CB of the right anterior implant region at 19.824913 N/mm², and the lowest in the CB of the right posterior implant region at 4.321727 N/mm² (Fig.3h) (Table 3).

Results of minimum principal stress in the cortical bone around the implant

When force was applied between two implants in a Cr-Co substructure with a composite superstructure, the lowest MinPS was observed in the CB of the left posterior implant region at -10.416149 N/mm², while the highest MinPS was observed in the CB of the right posterior implant region at -1.520808 N/mm² (Fig.4a) (Table 4). When force was applied to the cantilever portion of a the same combination, the lowest MinPS was observed in the CB of the left posterior implant region at -37.027302 N/mm², and the highest MinPS was observed in the CB of the right anterior implant region at -4.175044 N/mm² (Fig.4b) (Table 4).

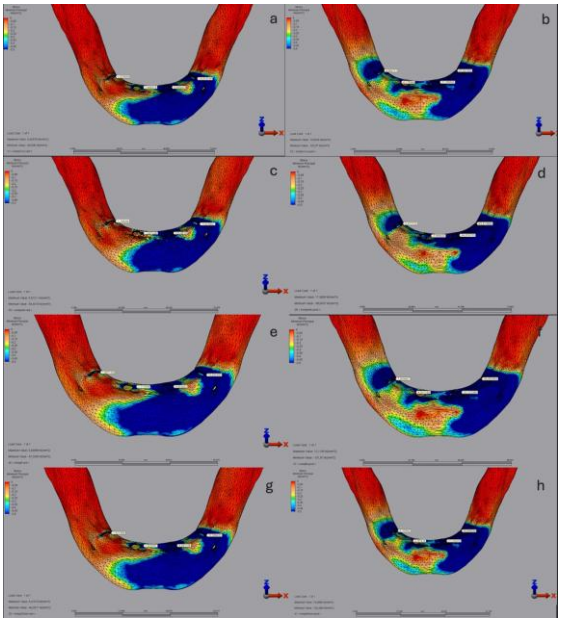

Figure 4. Composite Superstructure Minimum Principal Stress; (a, b) Cr-Co Substructure (a: anterior load, b: posterior load); (c, d) PEEK Substructure (c: anterior load, d: posterior load); (e, f) Titanium Substructure (e: anterior load, f: posterior load);(g, h) Zirconia Substructure (g: anterior load, h: posterior load).

In the PEEK substructure with a composite superstructure, when force was applied between the two implants, the lowest MinPS was observed in the CB of the left posterior implant region at -11.570927 N/mm², while the highest was found in the CB of the right anterior implant region at -1.091225 N/mm² (Fig.4c) (Table 4). When force was applied to the cantilever of the same combination, the lowest

Table 4. Minimum principal stress values (N/mm²) in the cortical bone around the implant for different substructure and superstructure combinations.

Combination	Anterior load – Right posterior implant	Anterior load – Right anterior implant	Anterior load – Left anterior implant	Anterior load – Left posterior implant	Posterior load – Right posterior implant	Posterior load – Right anterior implant	Posterior load – Left anterior implant	Posterior load – Left posterior implant
Cr-Co Substructure – Composite Superstructure	-1.520808	-1.806310	-9.500462	-10.416149	-8.065777	-4.175044	-21.296924	-37.027302
PEEK Substructure – Composite Superstructure	-1.759095	-1.091225	-9.574514	-11.570927	-4.372725	-2.999020	-34.074733	-43.813800
Titanium Substructure – Composite Superstructure	-1.487134	-1.711939	-9.552552	-10.632292	-7.509867	-4.031745	-23.222380	-38.483984
Zirconia Substructure – Composite Superstructure	-1.521998	-1.814261	-9.497125	-10.398420	-8.103502	-4.181418	-21.142418	-36.904036
Cr-Co Substructure – Zirconia Superstructure	-1.416865	-2.767117	-10.126320	-10.104143	-8.417940	-4.142041	-17.046186	-33.900477
PEEK Substructure – Zirconia Superstructure	-1.523301	-1.473468	-9.349499	-10.584618	-7.417029	-3.479953	-24.044234	-37.598654
Titanium Substructure – Zirconia Superstructure	-1.432913	-2.490632	-9.975522	-10.130849	-8.463309	-4.110895	-18.101710	-34.797301
Zirconia Substructure – Zirconia Superstructure	-1.415330	-2.787156	-10.136509	-10.114685	-8.408122	-4.140722	-16.966652	-33.819820

MEANDROS MEDICAL AND DENTAL JOURNAL
March 2025 (1):117-128

Meandros Medical and Dental Journal
doi: 10.69601/meandrosmdj.1603483

MinPS was observed in the CB of the left posterior implant region at -43.813800 N/mm², and the highest was found in the CB of the right anterior implant region at -2.999020 N/mm² (Fig.4d) (Table 4).

When force was applied between two implants in a titanium substructure with a composite superstructure, the lowest MinPS was observed in the CB of the left posterior implant region at -10.632292 N/mm², while the highest MinPS was observed in the CB of the right posterior implant region at -1.487134 N/mm² (Fig.4e) (Table 4). When force was applied to the cantilever of the same combination, the lowest MinPS was observed in the CB of the left posterior implant region at -38.483984 N/mm², and the highest MinPS was observed in the CB of the right anterior implant region at -4.031745 N/mm² (Fig.4f) (Table 4).

When force was applied between two implants in a zirconia substructure with a composite superstructure, the lowest MinPS was observed in the CB of the left posterior implant region at -10.398420 N/mm², while the highest MinPS was observed in the CB of the right posterior implant region at -1.521998 N/mm² (Fig.4g) (Table 4). When force was applied to the cantilever of the same combination, the lowest MinPS stress was observed in the CB of the left posterior implant region at -36.904036 N/mm², and the highest MinPS was observed in the CB of the right anterior implant region at -4.181418 N/mm² (Fig.4h) (Table 4).

When force was applied between two implants in a Cr-Co substructure with a zirconia superstructure, the lowest MinPS was observed in the CB of the left anterior implant region at -10.126320 N/mm², while the highest MinPS was observed in the CB of the right posterior implant region at -1.416865 N/mm² (Fig.5a) (Table 4). When force was applied to the cantilever of the same combination, the lowest MinPS was observed in the CB of the left posterior implant region at -33.900477 N/mm², and the highest MinPS was observed in the CB of the right anterior implant region at -4.142041 N/mm² (Fig.5b) (Table 4).

When force was applied between two implants in a PEEK substructure with a zirconia superstructure, the lowest MinPS was observed in the CB of the left posterior implant region at -10.584618 N/mm², while the highest MinPS was observed in the CB of the right anterior implant region at -1.416865 N/mm² (Fig.5c) (Table 4). When force was applied to the cantilever of the same combination, the lowest MinPS was observed in the CB of the left posterior implant region at -37.598654 N/mm², and the highest MinPS was observed in the CB of the right anterior implant region at -3.479953 N/mm² (Fig.5d) (Table 4).

When force was applied between two implants in a titanium substructure with a zirconia superstructure, the lowest MinPS was observed in the CB of the left posterior implant region at -10.130849 N/mm², while the highest MinPS was observed in the CB of the right posterior implant region at -1.432913 N/mm² (Fig.5e) (Table 4). When force was applied to the cantilever of the same combination, the lowest MinPS was observed in the CB of the left posterior implant region at -34.797301 N/mm², and the highest MinPS was observed in the CB of the right anterior implant region at -4.110895 N/mm² (Fig.5f) (Table 4).

When force was applied between two implants in a zirconia substructure with a zirconia superstructure, the lowest MinPS was observed in the CB of the left anterior implant region at -10.136509 N/mm², while the highest MinPS was observed in the CB of the right posterior implant region at -1.415330 N/mm² (Fig.5g) (Table 4). When force was applied to the cantilever of the same combination, the lowest MinPS was observed in the CB of the left posterior implant region at -33.819820 N/mm², and the highest MinPS was observed in the CB of the right anterior implant region at -4.140722 N/mm² (Fig.5h) (Table 4).

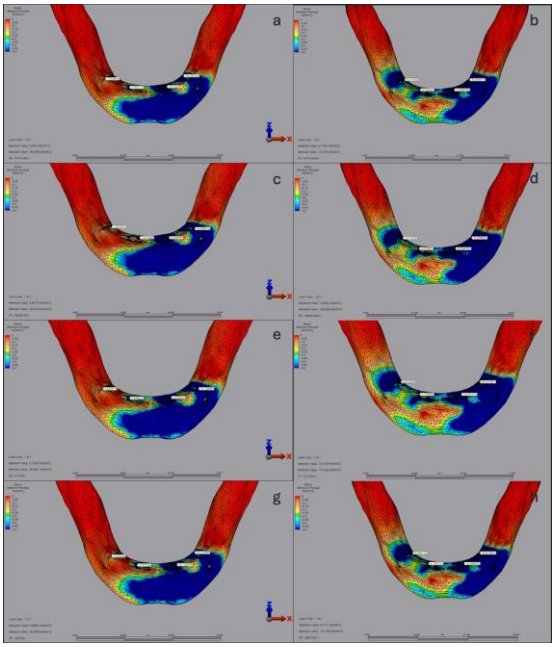

Figure 5. Zirconia Superstructure Minimum Principal Stress; (a, b) Cr-Co Substructure (a: anterior load, b: posterior load); (c, d) PEEK Substructure (c: anterior load, d: posterior load); (e, f) Titanium Substructure (e: anterior load, f: posterior load);(g, h) Zirconia Substructure (g: anterior load, h: posterior load).

MEANDROS MEDICAL AND DENTAL JOURNAL
March 2025 (1):117-128

Meandros Medical and Dental Journal
doi: 10.69601/meandrosmdj.1603483

DISCUSSION

The null hypothesis of the study "there is no difference in the effect of different substructure and superstructure materials used in All-on-4 prosthetic restorations on bone stress distribution" was rejected. In our study, different stress distributions in the bone were observed with different substructure and superstructure materials.

In implant-supported prostheses, the use of polymeric materials such as PEEK (polyether ether ketone), manufactured by CAD-CAM(Computer Aided Design-Computer Aided Manufacturing) milling, has been suggested as an alternative to high-elastic modulus, rigid materials like titanium, Cr-Co, and zirconia due to advantages like lower cost, light weight, and shock absorption (14,15). It is thought that PEEK substructures with an appropriate elastic modulus may be beneficial for patients with temporomandibular joint complaints (16). Some studies have shown that rigid, non-polymeric substructures with high elastic modulus do not absorb shock, thus transmitting more stress to the bone-implant interface (17). Zoidis argued that polymeric materials like PEEK, which can be milled using CAD-CAM, could be used instead of rigid substructures like Cr-Co, zirconia, or titanium (18). However, other studies have reported that using a rigid substructure provides better stress distribution and reduces stresses in the surrounding bone of the implant (19,20). There is limited information on the biomechanical behavior of polymeric and non-polymeric materials in implant-supported fixed prostheses and their effect on stress distribution in the surrounding bone(21). Oral microflora adhesion to PEEK surfaces is lower compared to zirconia, titanium, and PMMA.

There are some limitations in finite element analysis. The models used in this study are defined as linear elastic, homogeneous, and isotropic. While these assumptions are common in finite element analysis, the actual clinical behaviors cannot be fully simulated(7).

Modeling the mechanical behavior of cortical or trabecular bone is difficult because bone is highly anisotropic, heterogeneous, and depends on many parameters such as age, gender, and bone type. As a result, it is not easy to define the exact material properties of a specific bone being studied numerically. Therefore, in most finite element analyses, the mechanical properties of bone are assumed to be isotropic.

In finite element analysis studies, MaxPS is generally used to observe tensile stress, and minimum principal stress is used for compressive stress. Given the flexible and brittle response of bone, it is appropriate to use compressive stress/strain to analyze the biomechanical behavior of the bone surrounding the implant(22).

Using the same superstructure is used in all force applications, higher MaxPS values are observed in the CB surrounding the implants in the PEEK substructure group compared to the other substructure groups, in the direction of force. Applying force between implants produces the highest MaxPS is observed in the CB of the left anterior implant region. Under these conditions, a combination of PEEK substructure and composite superstructure yields a MaxPS value of 6.299223 N/mm² in the CB surrounding the left anterior implant region. Applying force to the cantilever section results lower MaxPS values are observed in the zirconia superstructure group compared to the composite superstructure group in the same substructure combinations. In all combinations where force is applied to the cantilever section, the highest MaxPS values are observed in the CB surrounding right anterior implant. Applying force to the cantilever section with the same superstructure material results in lower MaxPS values in the CB of the implant farthest from the force in the PEEK substructure group, compared to other substructure groups. The highest MaxPS value is observed in the CB surrounding the right anterior implant in the titanium substructure and zirconia superstructure combination, which is 19.868105 N/mm². The low Young's modulus of the PEEK substructure causes it to flex, generating more tensile stress in the CB near the force application site. Rigid substructures, on the other hand, absorb the force as a whole and transmit it to the opposing arch, creating a more homogeneous stress distribution with the opposite arch stabilizing the CB.

Using the same superstructure results in the lowest minimum principal stresses in all combinations in the CB surrounding the left posterior implant in the PEEK substructure group.

Force application to the cantilever section results in MinPS values in the CB following the order from lowest to highest as: left posterior implant region, left anterior implant region, right posterior implant region, and right anterior implant region.

Force application to the cantilever section also leads to MinPS values in the CB in the direction of force (left anterior and posterior implant regions) following the order from highest to lowest as: zirconia, Cr-Co, titanium, and PEEK. These values increase as the Young's Modulus increases(Young's Modulus: PEEK 4,200 MPa, Titanium 110,000 MPa, Cr-Co 200,000 MPa, Zirconia 210,000 MPa).

MEANDROS MEDICAL AND DENTAL JOURNAL
March 2025 (1):117-128

Meandros Medical and Dental Journal
doi: 10.69601/meandrosmdj.1603483

In combinations where force is applied to the cantilever section and the same substructure is used, the MinPS values in the composite superstructure are lower than in the zirconia superstructure.

When force is applied between two implants and the same substructure is used, the MinPS values in the CB of the left posterior implant region are lower in the composite superstructure compared to the zirconia superstructure. The compression values in the CB are concentrated in the region closest to the force. Higher stress peak values are observed in PEEK substructure and composite superstructure materials with low elastic modulus. The low elastic modulus of the PEEK substructure and composite superstructure material allows more compression forces to be transmitted to the CB closest to the force application site.

Some authors have mentioned the cushioning effect of PEEK material in stress transmission to the peri-implant region. Wang et al. stated that the combination of PEEK substructures and PMMA crowns could show an elastic cushioning effect under chewing forces compared to metal/zirconia substructures with high elastic moduli (16). Therefore, it was noted that metal/zirconia substructures might increase stress concentration in the alveolar crest between implants. Seemann et al. reported that the combination of PEEK substructures with resin superstructures could reduce the transmission of occlusal forces (23). Zoidis suggested that combining PEEK substructures with acrylic teeth, both with low elastic moduli, might act as stress breakers and reduce occlusal stresses (18). Conserva et al. reported that rigid substructures with high elastic moduli do not absorb shock, transmitting more stress to the implant-bone interface, potentially leading to prosthetic failures, bone and implant loss (17).

Other authors recommend using relatively rigid substructure materials to prevent failure. In the study by Bacchi et al., it was reported that using more rigid materials resulted in lower stress in the bone (24). In the in-vitro study by Sirandoni et al., it was found that, despite the cushioning effect of polymeric materials, stress reduction in the substructure occurred, but there was an increase in stress in the surrounding implant bone (21). This increase was attributed to the high elasticity of the material and the lack of a rigid substructure. In the study by Jaros et al., Ni-Cr and PEEK substructure bars were compared using finite element analysis in an All-on-4 design (11). Although both systems showed similar results in stress distribution in the surrounding bone under axial force, the PEEK bar system transmitted more stress to the implant surrounding bone under oblique forces. In the study by Kelkar et al., zirconia, titanium, and PEEK substructure materials in All-on-4 prostheses were evaluated using finite element analysis (8). In that study, the least displacement was observed with zirconia substructures, while similar values were observed for PEEK and titanium. Excessive micromovements at the implant-bone interface can have harmful effects. In the photo-elastic stress study by Çalışkan and Yöndem on All-on-4 prostheses, metal and zirconia showed lower stress values compared to PEEK (25). Based on these results, the authors suggested that an increase in the elastic modulus of the substructure material reduces the stress transmitted to the bone and implants. Our study found similar results to these conclusions. We believe that non-rigid substructures transmit more force to the implants in the region closest to the force application.

Limitations of the Study

Although we attempt to recreate intraoral structures in a computer environment using finite element analysis, intraoral conditions cannot be fully simulated, and long-term clinical studies are needed to support the data obtained from our study. The application of unidirectional and static force may not fully represent real-life conditions, and given the brittle nature of zirconia, different outcomes could be observed under cyclic loading, such as during chewing (4). The data obtained in our study should be supported by long-term clinical studies.

CONCLUSION

I. Higher tensile forces were observed in the cortical bone surrounding the implant in the direction of the applied force in the PEEK substructure and composite superstructure groups. In these groups, strain forces in the cortical bone surrounding the implant were higher in the direction of the force compared to the direction opposite to the force. Rigid substructures absorbed the strain forces as a whole and transmitted less force to the cortical bone in the direction of the applied force, while transmitting more force to the cortical bone in the opposite arch.

II. The compressive values in the cortical bone surrounding the implant were ranked by substructures from highest to lowest as follows: PEEK, titanium, Cr-Co, and zirconia. The low elastic modulus of the PEEK substructure and composite superstructure caused more compression forces to be transmitted to the cortical bone near the force application site due to their flexibility.

III. In the composite superstructure, higher stress accumulation values were observed in the cortical bone in

the direction of the applied force compared to the zirconia superstructure.

Acknowledgments
The authors declare that they have no acknowledgements to make.

Authorship contributions
EÇ conceived the study and wrote the manuscript. MEÇ provided guidance on structuring and editing the manuscript. MS guided the modeling and finite element analysis aspects of the study and also assisted with editing the manuscript. MHŞ assisted with editing the manuscript.

Data availibity statement
The data that support the findings of this study are available from the corresponding author upon reasonable request.

Declaration of competing interest
The authors declare that they have no conflict of interest.

Ethics
This study did not involve human participants, animals, or sensitive data, and therefore did not require ethical approval.

Funding
This research did not receive any specific grant from funding agencies in the public, commercial, or not-for-profit sectors.

REFERENCES
1. Horita S, Sugiura T, Yamamoto K, Murakami K, Imai Y, Kirita T. Biomechanical analysis of immediately loaded implants according to the "All-on-Four" concept. J Prosthodont Res. 2017 Apr;61(2):123–32.
2. Taruna M. Prosthodontic Perspective to All- On-4 ® Concept for Dental Implants. JOURNAL OF CLINICAL AND DIAGNOSTIC RESEARCH. 2014;
3. Babbush CA, Kutsko GT, Brokloff J. The All-on-Four immediate function treatment concept with nobelactive implants: A retrospective study. Vol. 37, Journal of Oral Implantology. 2011. p. 431–45.
4. Bhering CLB, Mesquita MF, Kemmoku DT, Noritomi PY, Consani RLX, Barão VAR. Comparison between all-on-four and all-on-six treatment concepts and framework material on stress distribution in atrophic maxilla: A prototyping guided 3D-FEA study. Mater Sci Eng C Mater Biol Appl. 2016 Dec 1;69:715–25.
5. Kupprano P, Kamonkhantikul K, Homsiang W, Takahashi H, Arksornnukit M. Finite element analysis on implant-supported bar with different geometric shapes. BMC Oral Health. 2024 Dec 30;24(1):1572.
6. Al Jabbari YS. Physico-mechanical properties and prosthodontic applications of Co-Cr dental alloys: a review of the literature. J Adv Prosthodont. 2014 Apr;6(2):138–45.
7. Dayan SC, Geckili O. The influence of framework material on stress distribution in maxillary complete-arch fixed prostheses supported by four dental implants: a three-dimensional finite element analysis. Comput Methods Biomech Biomed Engin. 2021 Nov;24(14):1606–17.
8. Kelkar KC, Bhat V, Hegde C. Finite element analysis of the effect of framework materials at the bone-implant interface in the all-on-four implant system. Dent Res J (Isfahan). 2021;18:1.
9. Jin HY, Teng MH, Wang ZJ, Li X, Liang JY, Wang WX, et al. Comparative evaluation of BioHPP and titanium as a framework veneered with composite resin for implant-supported fixed dental prostheses. J Prosthet Dent. 2019 Oct;122(4):383–8.
10. Takaba M, Tanaka S, Ishiura Y, Baba K. Implant-supported fixed dental prostheses with CAD/CAM-fabricated porcelain crown and zirconia-based framework. J Prosthodont. 2013 Jul;22(5):402–7.
11. Jaros OAL, De Carvalho GAP, Franco ABG, Kreve S, Lopes PAB, Dias SC. Biomechanical Behavior of an Implant System Using Polyether Ether Ketone Bar: Finite Element Analysis. J Int Soc Prev Community Dent. 2018;8(5):446–50.
12. Tribst JPM, de Morais DC, Alonso AA, Piva AM de OD, Borges ALS. Comparative three-dimensional finite element analysis of implant-supported fixed complete arch mandibular prostheses in two materials. J Indian Prosthodont Soc. 2017;17(3):255–60.
13. Kohorst P, Borchers L, Strempel J, Stiesch M, Hassel T, Bach FW, et al. Low-temperature degradation of different zirconia ceramics for dental applications. Acta Biomater. 2012 Mar;8(3):1213–20.
14. Maló P, de Araújo Nobre MA, Lopes A V, Rodrigues R. Immediate loading short implants inserted on low bone quantity for the rehabilitation of the edentulous maxilla using an All-on-4 design. J Oral Rehabil. 2015 Aug;42(8):615–23.
15. Seemann R, Wagner F, Marincola M, Ewers R. Fixed, Fiber-Reinforced Resin Bridges on 5.0-mm Implants in Severely Atrophic Mandibles: Up to 5 Years' Follow-Up of a Prospective Cohort Study. Journal of Oral and Maxillofacial Surgery. 2018 May;76(5):956–62.
16. Wang J, Wu P, Liu HL, Zhang L, Liu LP, Ma CF, et al. Polyetheretherketone versus titanium CAD-CAM framework for implant-supported fixed complete dentures: a retrospective study with up to 5-year follow-up. J Prosthodont Res. 2022 Apr 27;66(2):279–87.

17. Conserva E, Menini M, Tealdo T, Bevilacqua M, Ravera G, Pera F, et al. The use of a masticatory robot to analyze the shock absorption capacity of different restorative materials for prosthetic implants: a preliminary report. Int J Prosthodont. 2009;22(1):53–5.
18. Zoidis P. The all-on-4 modified polyetheretherketone treatment approach: A clinical report. J Prosthet Dent. 2018 Apr;119(4):516–21.
19. Zhang G, Yuan H, Chen X, Wang W, Chen J, Liang J, et al. A Three-Dimensional Finite Element Study on the Biomechanical Simulation of Various Structured Dental Implants and Their Surrounding Bone Tissues. Int J Dent. 2016;2016:1–9.
20. Pieri F, Aldini NN, Fini M, Corinaldesi G. Immediate Occlusal Loading of Immediately Placed Implants Supporting Fixed Restorations in Completely Edentulous Arches: A 1 - Year Prospective Pilot Study. J Periodontol. 2009 Mar;80(3):411 – 21.
21. Sirandoni D, Leal E, Weber B, Noritomi PY, Fuentes R, Borie E. Effect of Different Framework Materials in Implant-Supported Fixed Mandibular Prostheses: A Finite Element Analysis. Int J Oral Maxillofac Implants. 2019;34(6):e107–14.
22. Liu T, Mu Z, Yu T, Wang C, Huang Y. Biomechanical comparison of implant inclinations and load times with the all-on-4 treatment concept: a three-dimensional finite element analysis. Comput Methods Biomech Biomed Engin. 2019 May;22(6):585–94.
23. Seemann R, Marincola M, Seay D, Perisanidis C, Barger N, Ewers R. Preliminary results of fixed, fiber-reinforced resin bridges on four 4- × 5-mm ultrashort implants in compromised bony sites: a pilot study. J Oral Maxillofac Surg. 2015 Apr;73(4):630–40.
24. Bacchi A, Consani RLX, Mesquita MF, Dos Santos MBF. Effect of framework material and vertical misfit on stress distribution in implant-supported partial prosthesis under load application: 3-D finite element analysis. Acta Odontol Scand. 2013 Sep;71(5):1243–9.
25. ÇALIŞKAN A, YÖNDEM İ. Stress Analysis Of Fixed Dental Prostheses Produced With Different Materials According To The All-On-Four Concept. Journal of Biotechnology and Strategic Health Research. 2019 Dec 31;3(3):183–91.